ERJ Express. Published on April 13, 2016 as doi: 10.1183/13993003.01677-2015

ORIGINAL ARTICLE
IN PRESS | CORRECTED PROOF

Recurrent *NRAS* mutations in pulmonary Langerhans cell histiocytosis

Samia Mourah[1], Alexandre How-Kit[2], Véronique Meignin[3], Dominique Gossot[4], Gwenaël Lorillon[5], Emmanuelle Bugnet[5], Florence Mauger[6], Celeste Lebbe[7], Sylvie Chevret[8,9], Jörg Tost[6] and Abdellatif Tazi[5,9]

Affiliations: [1]Assistance Publique – Hôpitaux de Paris, Laboratoire de Pharmacologie Biologique, Hôpital Saint-Louis; Université Paris-Diderot, Sorbonne Paris Cité; INSERM U976, Paris, France. [2]Laboratoire de Génomique fonctionnelle, Fondation Jean Dausset – CEPH, Paris, France. [3]Assistance Publique – Hôpitaux de Paris, Service de Pathologie, Hôpital Saint-Louis; INSERM UMR_S1165, Paris, France. [4]Département Thoracique, Institut Mutualiste Montsouris, Paris, France. [5]Assistance Publique – Hôpitaux de Paris, Centre National de Référence de l'Histiocytose Langerhansienne, Service de Pneumologie, Hôpital Saint-Louis, Paris, France. [6]Laboratoire Epigénétique et Environnement, Centre National de Génotypage, CEA-Institut de Génomique, Evry, France. [7]Assistance Publique – Hôpitaux de Paris, Département de Dermatologie, Hôpital Saint-Louis; Université Paris-Diderot, Sorbonne Paris Cité; INSERM U976, Paris, France. [8]Assistance Publique – Hôpitaux de Paris; Service de Biostatistique et Information Médicale, Hôpital Saint-Louis, Paris, France. [9]Université Paris-Diderot, Sorbonne Paris Cité; INSERM UMR 1153 CRESS, Equipe de Recherche en Biostatistiques et Epidémiologie Clinique, Paris, France.

Correspondence: Abdellatif Tazi, Service de Pneumologie, Hôpital Saint-Louis, 1 Avenue Claude Vellefaux, 75475, Paris cedex 10, France. E-mail: abdellatif.tazi@sls.aphp.fr

ABSTRACT The mitogen-activated protein kinase (MAPK) pathway is constantly activated in Langerhans cell histiocytosis (LCH). Mutations of the downstream kinases *BRAF* and *MAP2K1* mediate this activation in a subset of LCH lesions. In this study, we attempted to identify other mutations which may explain the MAPK activation in nonmutated *BRAF* and *MAP2K1* LCH lesions.

We analysed 26 pulmonary and 37 nonpulmonary LCH lesions for the presence of *BRAF*, *MAP2K1*, *NRAS* and *KRAS* mutations. Grossly normal lung tissue from 10 smoker patients was used as control. Patient spontaneous outcomes were concurrently assessed.

$BRAF^{V600E}$ mutations were observed in 50% and 38% of the pulmonary and nonpulmonary LCH lesions, respectively. 40% of pulmonary LCH lesions harboured $NRAS^{Q61K/R}$ mutations, whereas no *NRAS* mutations were identified in nonpulmonary LCH biopsies or in lung tissue control. In seven out of 11 $NRAS^{Q61K/R}$-mutated pulmonary LCH lesions, $BRAF^{V600E}$ mutations were also present. Separately genotyping each CD1a-positive area from the same pulmonary LCH lesion demonstrated that these concurrent *BRAF* and *NRAS* mutations were carried by different cell clones. $NRAS^{Q61K/R}$ mutations activated both the MAPK and AKT (protein kinase B) pathways. In the univariate analysis, the presence of concurrent $BRAF^{V600E}$ and $NRAS^{Q61K/R}$ mutations was significantly associated with patient outcome.

These findings highlight the importance of *NRAS* genotyping of pulmonary LCH lesions because the use of BRAF inhibitors in this context may lead to paradoxical disease progression. These patients might benefit from MAPK kinase inhibitor-based treatments.

@ERSpublications
Pulmonary Langerhans cell histiocytosis genetic landscape includes recurrent activating *NRAS* Q61 mutations http://ow.ly/YgsSm

This article has supplementary material available from erj.ersjournals.com

Received: Oct 09 2015 | Accepted after revision: Feb 11 2016

Support statement: The authors acknowledge support from Legs Poix (Chancellerie des Universités) and the Fonds de Dotation Recherche en Santé Respiratoire. Funding information for this article has been deposited with FundRef.

Conflict of interest: Disclosures can be found alongside the online version of this article at erj.ersjournals.com

Introduction

Langerhans cell histiocytosis (LCH) is a rare disorder of unknown origin that encompasses a large clinical spectrum [1]. Lung involvement is frequently observed in young adult smokers and exhibits variable outcomes [2–4]. Alterations in the mitogen-activated protein kinase (MAPK) pathway are involved in the pathogenesis of LCH [5]. The MAPK pathway is critical for oncogenic signalling and results from the activation of growth factor receptors, leading to cell proliferation and survival. The MAPK pathway is initiated with the activation of RAS, which then stimulates the downstream kinases RAF, the MAPK kinase (MEK1/2) and extracellular signal-regulated kinase (ERK1/2) [5] (online supplementary figure S1). Somatic activating $BRAF^{V600E}$ mutations are identified in LCH lesions in 30–60% of cases, including pulmonary LCH (PLCH) [6–12]. *BRAF*-activating mutations have generated interest in the use of BRAF inhibitor (BRAFi) treatment in progressive cases of LCH [5, 6, 13]. Importantly, the MEK/ERK pathway is activated independently of the lesion's *BRAF* status, indicating that other mechanisms could be involved in MAPK pathway activation in LCH [6]. More recently, mutations in *MAP2K1* (a member of the MEK family) were identified in 15–50% of *BRAF* wild-type (WT) nonpulmonary LCH lesions, thereby explaining MAPK pathway activation in these cases [14–16]. Individual cases of other mutations in the MAPK pathway have also been reported [15, 17]. However, additional mechanisms remain to be identified to explain the MAPK pathway activation in the substantial subset of LCH lesions in which no mutation has been identified.

Mutations in the RAS family, small GTPases upstream of MEK/ERK, are able to activate the MAPK pathway [18]. We therefore screened for the presence of *NRAS*- and *KRAS*-activating mutations in a series of lung LCH biopsies, and compared the results with those obtained in nonpulmonary LCH lesions. Strikingly, whereas no *NRAS* mutations were present in the nonpulmonary LCH lesions, we identified $NRAS^{Q61K/R}$ mutations in a significant subset of PLCH lesions. We also evaluated their functional consequences and sought an association with patient outcome.

TABLE 1 Clinical characteristics of the 26 patients with pulmonary Langerhans cell histiocytosis whose surgical lung biopsies were analysed

At diagnosis	
Age years	32 (27–44)
Female	13 (50)
Current smokers	26 (100)
Pack-years	16 (7–26)
Dyspnoea	16 (61)
NYHA II/III/IV	9/5/2
Pneumothorax	8 (31)
Lung function	
TLC % pred	96.8±12.0
FVC % pred	86.7±20.1
RV % pred	123.9±43.3
RV/TLC % pred	125±38.8
FEV_1 % pred	83.6±20.7
FEV_1/FVC %	80.3±10.7
D_{LCO} % pred[#]	61.2±14.7
During follow-up	
Follow-up duration months	41 (26–84)
Outcome status[¶]	
Persistent smoking	14 (54)
Improvement	5 (35.7)
Stability	2 (14.3)
Deterioration	7 (50)
Smoking cessation	12 (46)
Improvement	8 (66.7)
Stability	2 (16.7)
Deterioration	2 (16.7)

Data are presented as median (interquartile range), n (%) or mean±SD. PLCH: pulmonary Langerhans cell histiocytosis; NYHA: New York Heart Association; TLC: total lung capacity; FVC: forced vital capacity; RV: residual volume; FEV_1: forced expiratory volume in 1 s; D_{LCO}: diffusing capacity of the lung for carbon monoxide. [#]: n=19; [¶]: outcome status was assessed at the last time of follow-up based on the variations of dyspnoea (NYHA stage) and lung function. A variation ⩾10% of FVC or FEV_1 or ⩾15% of D_{LCO} was considered significant.

DOI: 10.1183/13993003.01677-2015

Materials and methods

LCH biopsies

26 surgical lung biopsies from patients with PLCH were evaluated. The characteristics of these patients at diagnosis and during follow-up are presented in table 1. The outcomes of PLCH were assessed at the last available follow-up, and the patients were classified as improved or having persistent (stable) or progressive disease based on the variations of dyspnoea (assessed by New York Heart Association (NYHA) stage) and lung function as previously described [4]. No patient received any treatment for pulmonary LCH. 37 nonpulmonary LCH biopsies obtained from patients with isolated or multisystem disease were also studied. For five patients, two sites of biopsies were available (lung and another site n=4, bone and lymph node n=1). The characteristics of the entire study population of LCH patients are presented in online supplementary table S1.

The study was performed in accordance with the Helsinki Declaration and was approved by the INSERM Institutional Review Board and Ethics Committee in Paris (13-130), France. All patients provided informed consent.

Processing of LCH tissues

Formalin-fixed, paraffin-embedded (FFPE) biopsies were evaluated for the presence CD1a-positive nodules that were macrodissected for molecular biology analysis. To ensure that CD1a-positive cells were consistently present in the analysed specimens, CD1a immunostaining was performed every 10 consecutive tissue sections.

Lung tissue control

In cases in which the PLCH lesion was well circumscribed, the surrounding lung tissue containing <1% of CD1a-positive cells was evaluated as an internal control.

Grossly normal lung tissue from 10 patients who were smokers (six males, median (interquartile range (IQR)) age 64 (59–68) years) was obtained at the time of thoracic surgery for localised lung carcinoma (adenocarcinoma n=9, squamous cell carcinoma n=1) and was also analysed. Under light microscopy, these specimens exhibited mild fibrotic changes in the alveolar walls, accumulation of pigment-laden macrophages and alveolar epithelial hyperplasia.

Molecular analysis

DNA was extracted using the QIAamp DNA FFPE Tissue Kit for FFPE tissue from five 10-µm sections (Qiagen, Les Ulis, France) according to the manufacturer's protocol. DNA was qualified using a NanoDrop ND-1000 spectrophotometer (NanoDrop Technologies, Wilmington, DE, USA) and quantified using a Qubit® 2.0 fluorometer (Life Technologies, Saint-Aubin, France).

BRAF, *NRAS* and *KRAS* genotyping was performed using pyrosequencing, high-resolution melting (HRM) and enhanced *ice*-COLD-PCR (improved and complete enrichment coamplification at lower denaturation temperature PCR; E-*ice*-COLD-PCR) [19, 20]. *MAP2K1* genotyping was performed using Sanger sequencing [14].

Pyrosequencing

Mutation detection, identification and quantification were performed by genotyping using a PyroMark-Q96 MD pyrosequencer (Qiagen, Hilden, Germany). PCR products were purified and rendered single-stranded using a PyroMark-Q96 Vacuum Workstation (Qiagen) [19].

High-resolution melting

BRAF and *NRAS* HRM analyses were conducted according to the manufacturer's protocol using an LC480 HRM Scanning Master on a LightCycler 480 (Roche, Boulogne-Billancourt, France) [19].

E-ice-COLD-PCR

The sensitive detection of mutations in *NRAS* codons 12, 13 and 61, *BRAF* codon 600, and *KRAS* codons 12 and 13 by E-*ice*-COLD-PCR was performed in a LightCycler 480 (Roche Applied Science, Penzberg, Germany). The reaction contained 20 nM *BRAF* V600, 50 nM *NRAS* Q61 or 40 nM *KRAS* G12 and G13 blocker probes [19–21]. For *NRAS* G12 and G13 assay, 200 nM forward (AATTAACCCTGATTACTG) and reverse (biotin-GGATCATATTCATCTACAA) primers, 2 µM SYTO9 and 20 nM blocker probe (GCGCTTTTCCCAAC+A+C+C+A+C+CTGCTCCAAC-phosphate) were used.

Mutation detection, identification and quantification were performed by pyrosequencing. The mutant allele frequency (*i.e.* relative frequency of an allele) was expressed as a percentage. The limit of detection was evaluated at 0.1% of the mutant allele. The percentage of mutation of each sample was estimated after

mutation enrichment through E-*ice*-COLD-PCR using a standard curve including the following fractions of mutations: 5%, 1%, 0.5% and 0.1% (cell lines used: G-361 for *BRAF*, SW480 for *KRAS*, HL-60 for *NRAS* codon 61 and THP-1 for *NRAS* codon 12/13).

Sanger sequencing

MAP2K1 genotyping was performed using bidirectional Sanger sequencing of exons 2 and 3, as described by Brown *et al.* [14]. DNA was sequenced using a BigDye Terminator version 1.1 sequencing kit (Applied Biosystems, Foster City, CA, USA) and a 3130xl DNA analyser (Applied Biosystems).

Immunohistochemistry

The following monoclonal antibodies were used in this study: anti-CD1a (clone O10; Dako, Eching, Germany), anti-$BRAF^{V600E}$ (clone VE1; Spring Biosciences, Pleasanton, CA, USA), anti-phospho-ERK (pERK)-1/2 (clone MAPK-YT; Sigma, Lyon, France) and anti-phosphorylated protein kinase B (phospho-AKT) (Ser473) (clone D9E-XP; Cell Signaling, Saint Quentin Yvelines, France). The recently described $NRAS^{Q61R}$ antibody (clone SP174; Spring Biosciences) was used to assess the expression of $NRAS^{Q61R}$ protein [22]. $BRAF^{V600E}$- and $NRAS^{Q61K/R}$-mutated melanomas were used as positive controls.

Immunoglobulin isotype controls were used to assess nonspecific binding. Immunohistochemistry (IHC) was performed on serial sections as previously described [23] using Vectastain ABC-alkaline phosphatase or peroxidase systems (Vector, Burlingame, CA, USA). For pERK expression, a semiquantitative staining score, graded from – (absent) to +++ (strongly positive), was derived for each sample by comparing the staining intensity of CD1a-positive cells to the most intensely stained melanoma used as a positive control. The VE1 antibody staining was scored positive when viable tumour cells showed a clear cytoplasmic staining. Isolated nuclear staining, weak staining of single interspersed cells, faint diffuse staining or staining of monocytes/macrophages was considered negative [24]. The immunostaining scoring was performed by an experienced pathologist (V.M.) who had no knowledge of the mutational status of the lesions.

Immunofluorescence

Anti-CD1a antibody was applied to FFPE PLCH tissue sections followed by Alexa Fluor 568-conjugated donkey anti-mouse antibody (Life Technologies). Subsequently, anti-$NRAS^{Q61R}$ antibody was applied, followed by Alexa Fluor 488-conjugated goat anti-rabbit antibody (Life Technologies). Nuclei were counterstained using 4,6-diamidino-2-phenylindole (DAPI; Vector). Images were obtained using laser scanning confocal microscopy (Leica-Lasertechnik, Heidelberg, Germany).

In situ *proximity ligation assay*

Tissue sections were subjected to *in situ* proximity ligation assay (PLA) using a Duolink Detection kit (Olink Bioscience, Uppsala, Sweden) according to the manufacturer's instructions as previously described [25]. Briefly, slides were blocked, incubated with antibodies directed against CRAF (CliniSciences, Nanterre, France) and BRAF (Santa Cruz Biotechnology, Nanterre, France), and thereafter incubated with PLA probes, which are secondary antibodies (anti-mouse and anti-rabbit) conjugated to unique oligonucleotides. Circularisation and ligation of the oligonucleotides was followed by an amplification step. In this assay, a pair of oligonucleotide-labelled secondary antibodies (PLA probes) generates a signal only when bound in close proximity, thus allowing the detection of protein–protein interactions. Protein complexes were visualised as bright fluorescent signals (red dots) using a laser scanning confocal microscope (Leica-Lasertechnik). For quantification of PLA signals, the number of red dots per nuclei (DAPI signal) was counted (more than three fields) using ImageJ software (http://imagej.nih.gov/ij/) and a minimum number of three pictures per lesion were analysed [26].

Statistical analysis

Descriptive summary statistics, *i.e.* percentages for categorical variables, mean±SD or median (IQR) values for quantitative variables, were computed. A Kruskal–Wallis test was performed to compare the distribution of PLA dots according to mutation status. The comparison of patient outcome category (improved, stable or progressive disease) according to persistent or smoking cessation during follow-up was performed using the exact Fisher test.

The predictive value of patient characteristics at diagnosis, including *BRAF* and *NRAS* mutations, on patient outcomes (distinguishing improvement *versus* nonimprovement) was assessed by univariate and multivariable logistic regression models, where the strength of the association between each characteristic and the outcome was measured by the odds ratios (95% CI). Multivariable models included all variables associated with the outcome based on univariate analyses at the 10% level. Only those variables retained by a stepwise selection procedure were selected, at the 5% level.

DOI: 10.1183/13993003.01677-2015

All statistical analyses were performed using SAS version 9.3 (SAS, Cary, NC, USA) and R version 3.0.2 (www.R-project.org).

Results

BRAF *and* MAP2K1 *status of PLCH lesions*

The characteristics of the PLCH patients enrolled in the study are presented in table 1. *BRAF*^{V600E} was detected by pyrosequencing and E-*ice*-COLD PCR in 13 (50%) out of 26 of the samples within CD1a-positive cell-enriched areas (table 2). BRAF^{V600E} protein was also identified by IHC in 11 (85%) out of 13 *BRAF*^{V600E}-mutated cases detected by genotyping (figure 1 and table 2).

As *MAP2K1* mutations that were mutually exclusive with *BRAF*^{V600E} mutation were identified in nonpulmonary LCH lesions [14–16], we tested for the presence of these mutations in PLCH lesions. Among the 13 *BRAF* WT PLCH lesions, three (23%) specimens exhibited the *MAP2K1*^{C121S} mutation (table 2).

The MAPK pathway was activated in all analysed cases, although at a variable intensity, as assessed by pERK IHC (table 2 and online supplementary figure S2).

NRAS *mutations in PLCH lesions*

Given that MAPK pathway activation was also observed in *BRAF* and *MAP2K1* WT tissues, we evaluated whether PLCH lesions contain somatic mutations in the *NRAS* or *KRAS* oncogenes, potentially explaining MAPK activation. The 26 PLCH lesions were screened for *NRAS* G12/13 and Q61 and *KRAS* G12/13 mutations using pyrosequencing and HRM analysis. Among the 26 PLCH lesions, four cases exhibited a

TABLE 2 Phospho-extracellular signal-regulated kinase (pERK) and *BRAF*/*NRAS*/*MAP2K1* mutation status in the 26 analysed pulmonary Langerhans cell histiocytosis lesions

Patient	CD1a cells	pERK status[#]	*BRAF* V600 status			*MAP2K1* status	*NRAS* Q61 status	
			Genotype[¶]	Mutant allele frequency	VE1	Genotype	Genotype[¶]	Mutant allele frequency
1	30	+	*V600E*	36.7	+	WT	WT	0
2	40	2+	*V600E*	20.7	+	WT	WT	0
3	20	+	*V600E*	7.4	+	WT	*Q61K*	4.0
4	80	+++	*V600E*	8.9	+	WT	*Q61K*	5.2
5	80	–/+	*V600E*	29.6	+	WT	WT	0
6	50	–/+	*V600E*	16.1	+	WT	WT	0
7	20	++	*V600E*	9.2	+	WT	*Q61R*	39.1
8	50	+	*V600E*	7.6	–	WT	WT	0
9	20	+	*V600E*	19.4	+	WT	*Q61K*	2.0
10	10	–/+	*V600E*	12.0	+	WT	*Q61R*	1.0
11	40	+	*V600E*	16.3	–	WT	WT	0
12	30	+	*V600E*	27.9	+	WT	*Q61R*	1.0
13	50	++	*V600E*	10.5	+	WT	*Q61K*	8.3
14	10	+	WT	0	–	*C121S*	WT	0
15	50	+	WT	0	–	WT	WT	0
16	30	+/++	WT	0	–	WT	WT	0
17	50	++	WT	0	–	WT	WT	0
18	30	+	WT	0	–	WT	*Q61K*	4.0
19	40	+	WT	0	–	*C121S*	WT	0
20	10	NA	WT	0	NA	WT	WT	0
21	20	–/+	WT	0	+	WT	WT	0
22	10	NA	WT	0	–	WT	*Q61K*	1.0
23	10	NA	WT	0	NA	WT	*Q61K*	7.9
24	30	+	WT	0	–	*C121S*	WT	0
25	10	++	WT	0	–	WT	*Q61K*	3.0
26	30	+	WT	0	–	WT	WT	0

Data are presented as %, unless otherwise stated. WT: wild-type; NA: not available. [#]: two *BRAFV*^{600E}-mutated melanomas (both positive for VE1 immunostaining) were used as positive controls (these samples were scored ++ and +++, respectively, for pERK immunostaining); [¶]: *BRAF* and *NRAS* genotyping was performed by both pyrosequencing and E-*ice*-COLD-PCR (enhanced improved and complete enrichment coamplification at lower denaturation temperature PCR).

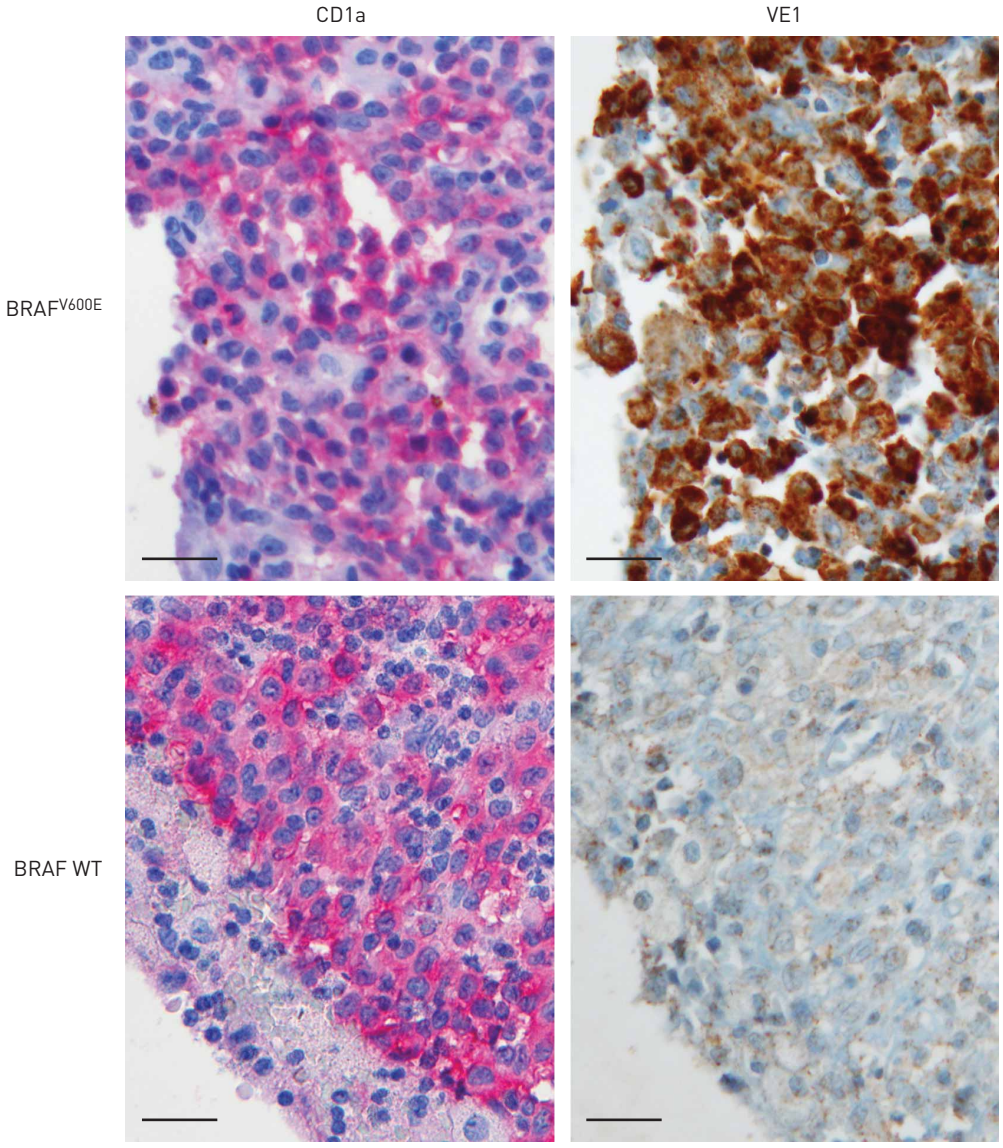

FIGURE 1 Immunostaining on serial tissue sections of the same specimens. Expression of CD1a and VE1 in a *BRAF*^{V600E}-mutated (patient 1) and in a *BRAF* wild-type (WT) (patient 17) pulmonary Langerhans cell histiocytosis (PLCH) specimen. Scale bar: 20 µm. 26 PLCH lesions were analysed.

NRAS$^{Q61R/K}$ mutation. Using E-*ice*-COLD-PCR, clonal *NRAS* Q61 mutations were identified in seven additional cases, which were *NRAS* WT using standard techniques. Thus, *NRAS* mutations were observed in 11 (42%) out of 26 PLCH lesions (table 2). In contrast, none of the PLCH lesions exhibited a *NRAS* G12 or G13 mutation, and only one lesion was positive for the *KRAS* G12S mutation (patient 15), although at the limit level of detection by E-*ice*-COLD-PCR.

For six PLCH specimens, the LCH lesion was well circumscribed and the surrounding lung tissue contained <1% CD1a-positive cells. Among these specimens, two PLCH lesions harboured a *NRAS*^{Q61K} and a *NRAS*^{Q61R} mutation, respectively. Interestingly, no *NRAS* mutation was detected in the surrounding lung tissue of these two specimens, even by E-*ice*-COLD-PCR.

To further demonstrate that the *NRAS*^{Q61R} mutation was specifically harboured by LCH CD1a-positive cells, we performed serial immunostaining on sections as well as double immunofluorescence and confocal microscopy with the recently described antibody against NRAS^{Q61R} protein [22]. As shown in figure 2, we could demonstrate specific NRAS^{Q61R} protein immunostaining by CD1a-positive cells in *NRAS*^{Q61R}-mutated PLCH lesions.

As *NRAS* mutations were not described in nonpulmonary LCH lesions, we tested for the presence of these mutations in 19 bone, 13 skin and five lymph node LCH biopsies. *NRAS* mutations were not detected in

DOI: 10.1183/13993003.01677-2015

any case, not even by E-*ice*-COLD-PCR. In contrast, *BRAF*^{V600E}mutations were identified in 38% of these specimens. Strikingly, among the four patients for whom both a lung biopsy and a nonpulmonary LCH tissue specimen were available, one patient (patient 25; table 2) harboured an *NRAS*^{Q61K} mutation in his PLCH lesion, whereas his cutaneous LCH lesion was *NRAS* WT.

Finally, because PLCH occurs almost exclusively in smokers, we also genotyped 10 control lung tissue specimens from patients who were smokers to evaluate the role of smoking *per se* on the eventual presence of *NRAS* mutations in the lung. No *NRAS* mutations were detected in any of these specimens.

Concurrent BRAF^{V600E} *and* NRAS$^{Q61K/R}$ *mutations in pulmonary LCH lesions*

Among the 11 *NRAS*-mutated PLCH lesions, seven harboured both *BRAF*^{V600E} and *NRAS*$^{Q61K/R}$ mutations with observed allele frequencies favouring the presence of clonal heterogeneity in these lesions (table 2). In contrast, no *MAP2K1* concurrent mutation was observed in the *NRAS*-mutated PLCH lesions (table 2).

To further examine whether *BRAF*^{V600E} and *NRAS*$^{Q61K/R}$ concurrent mutations found in the same PLCH specimens were the result of different histiocyte clones, we analysed a second lung biopsy block in five of these cases by separately genotyping each CD1a-positive area. In these cases, each focal CD1a-positive area within the same specimen harboured either *BRAF*^{V600E} or *NRAS*$^{Q61K/R}$ alone, or both mutations (figure 3 and table 3). Interestingly, in three of the five cases, whereas *NRAS*$^{Q61K/R}$ mutations were initially detected only by E-*ice*-COLD-PCR, these mutations were identified by pyrosequencing in separately genotyped CD1a-positive areas (tables 2 and 3). These findings strongly suggest that the concurrent *BRAF*^{V600E} and *NRAS*$^{Q61K/R}$ mutations identified in seven of 26 (27%) PLCH lesions are subclonal (*i.e.* not present in the entire population of tumour cells) and are carried by different CD1a-positive clonal populations.

Functional consequences of NRAS *mutations in PLCH lesions*

NRAS-activating mutations have been shown to induce BRAF and CRAF heterodimerisation, leading to MAPK pathway activation [27]. Using *in situ* PLA with a combination of CRAF and BRAF antibodies, we could detect a strong heterodimerisation (expressed as median (IQR) number of red dots per nuclei) in PLCH lesions harbouring *NRAS*$^{Q61K/R}$ mutations: either alone (32 (21–41); n=3, patients 22, 23 and 25) or concurrent with *BRAF*^{V600E} mutation (38 (30–47); n=3, patients 3, 4 and 7), as compared with *BRAF*^{V600E}/

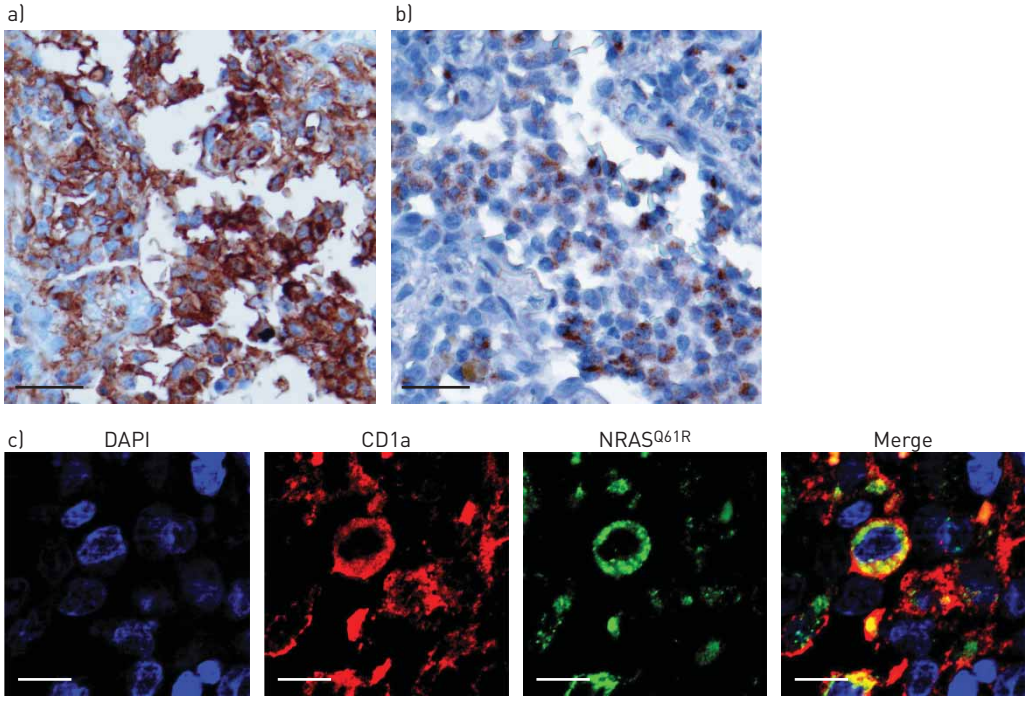

FIGURE 2 Expression of NRAS^{Q61R} protein in *NRAS*^{Q61R}-mutated pulmonary Langerhans cell histiocytosis (PLCH) lesions. a) Expression of CD1a and b) immunostaining with anti-NRAS^{Q61R} protein antibody performed on serial tissue sections. Scale bar: 30 µm. c) Confocal microscopy images of immunofluorescence staining of an *NRAS*^{Q61R}-mutated PLCH lesion stained with 4,6-diamidino-2-phenylindole (DAPI) (blue), anti-CD1a (red) and anti-NRAS^{Q61R} antibody (green), and a merged image of all three stains. Scale bar: 20 µm. All panels show representative images of the two *NRAS*^{Q61R}-mutated lesions (patients 7 and 10).

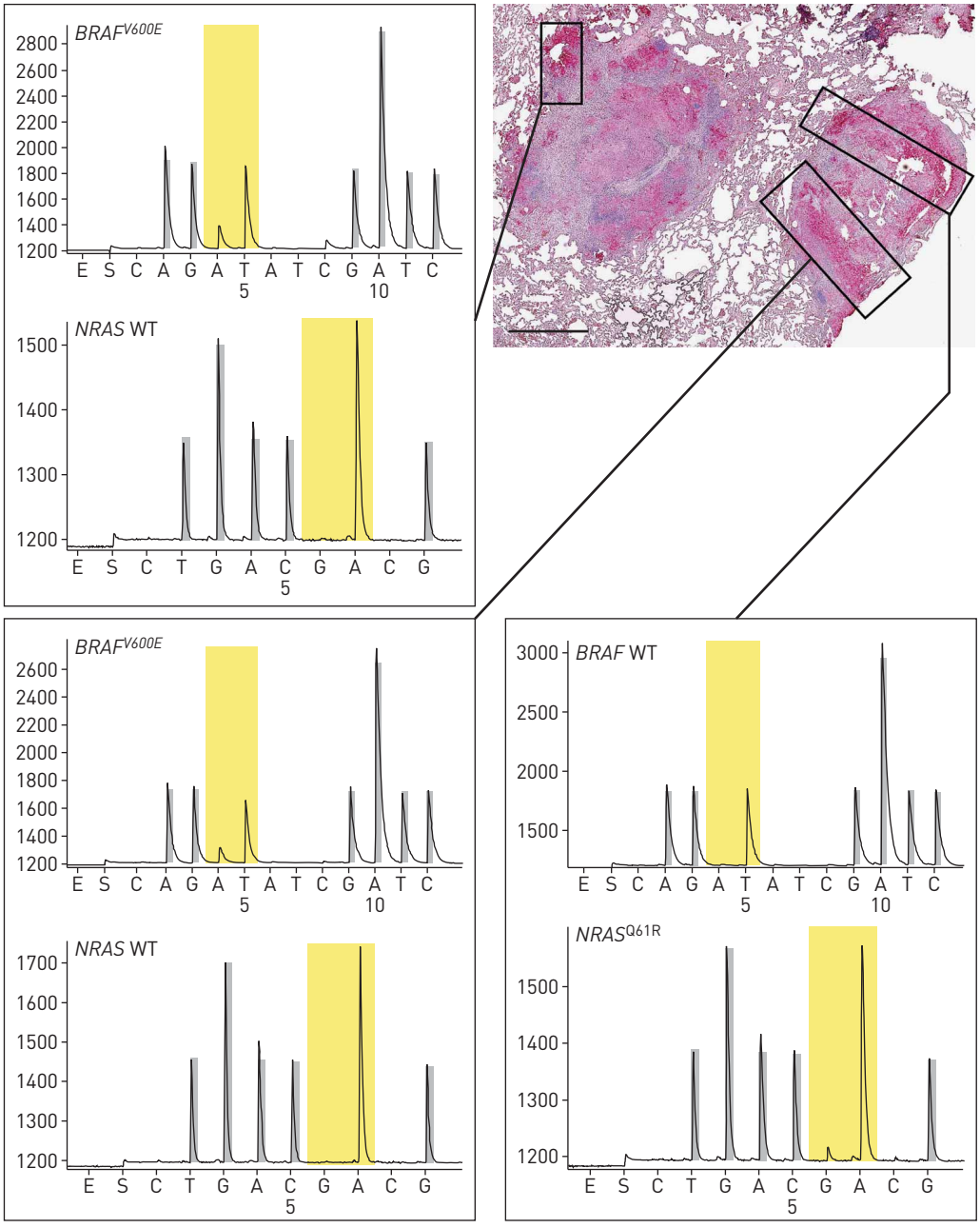

FIGURE 3 *BRAF* V600/*NRAS* Q61 clonal heterogeneity in pulmonary Langerhans cell histiocytosis (PLCH) lesions. Different CD1a-positive areas were separately genotyped for *BRAF* and *NRAS* mutations (patient 10). Pyrograms of $BRAF^{V600E}$ and $NRAS^{Q61R}$ mutations. Each sequence is derived from the corresponding lesion area. The different CD1a-positive areas from three PLCH lesions (patients 7, 10 and 12) were analysed. Scale bar: 1.5 mm.

NRAS WT (11 (3–14); n=3, patients 1, 5 and 6) or *BRAF* WT/*NRAS* WT (2 (2–3); n=3, patients 15, 17 and 20) lesions (p<0.0001; figure 4 and online supplementary figure S3).

As oncogenic RAS is a potential phosphatidylinositide 3-kinase/AKT signalling axis activator [28, 29], we assessed by IHC the AKT status in four PLCH lesions harbouring an *NRAS* Q61 mutation alone. AKT pathway activation was observed in all analysed cases, although with variable intensity (online supplementary figure S4).

Association of NRAS *mutations with clinical outcomes*

The amount of smoking (pack-years) did not correlate with the presence of *NRAS* mutations (p=0.67). 12 PLCH patients (46%) stopped smoking during follow-up (table 1). However, although a higher proportion

DOI: 10.1183/13993003.01677-2015

TABLE 3 Genotyping of separate CD1a-positive areas in pulmonary Langerhans cell histiocytosis specimens harbouring concurrent *BRAF*^{V600E} and *NRAS*$^{Q61K/R}$ mutations

Patient	CD1a area number	*BRAF* V600 status			*NRAS* Q61 status		
		Pyrosequencing	E-*ice*-COLD PCR	Mutant allele frequency	Pyrosequencing	E-*ice*-COLD PCR	Mutant allele frequency
7	1	*V600E*	*V600E*	25.7	*Q61R*	*Q61R*	26.1
	2	WT	WT	0	*Q61R*	*Q61R*	10.6
	3	*V600E*	*V600E*	21.8	WT	WT	0
	4	*V600E*	*V600E*	33.5	*Q61R*	*Q61R*	11.1
9	1	WT	*V600E*	1.0	*Q61K*	*Q61K*	7.8
10	1	*V600E*	*V600E*	18.8	WT	WT	0
	2	*V600E*	*V600E*	17.7	WT	WT	0
	3	WT	WT	0	*Q61R*	*Q61R*	13.5
12	1	*V600E*	*V600E*	35.3	*Q61R*	*Q61R*	6.7
	2	WT	WT	0	WT	WT	0
13	1	*V600E*	*V600E*	8.2	*Q61K*	*Q61K*	8.0

Data are presented as %, unless otherwise stated. E-*ice*-COLD-PCR: enhanced improved and complete enrichment coamplification at lower denaturation temperature PCR; WT: wild-type.

of patients who stopped smoking improved, this difference in the distribution of the outcomes of PLCH according to smoking status during follow-up was not statistically significant (p=0.24).

In the univariate analyses, there was no association between the presence of *BRAF*^{V600E} mutation alone and the patient outcome (p=0.24; table 4). Four variables were associated with the occurrence of spontaneous improvement of PLCH during follow-up at the 10% level, either positively for NYHA stage of dyspnoea (p=0.08) or negatively for forced expiratory volume in 1 s (FEV_1) (p=0.10), the presence of an *NRAS*$^{Q61K/R}$ mutation (p=0.05), and the presence of both *NRAS*$^{Q61K/R}$ and *BRAF*^{V600E} mutations (p=0.048). However, in the multivariate analysis, after incorporating the NYHA stage of dyspnoea and the FEV_1 at baseline, the presence of both *NRAS*$^{Q61K/R}$ and *BRAF*^{V600E} mutations was no longer statistically significant (p=0.07).

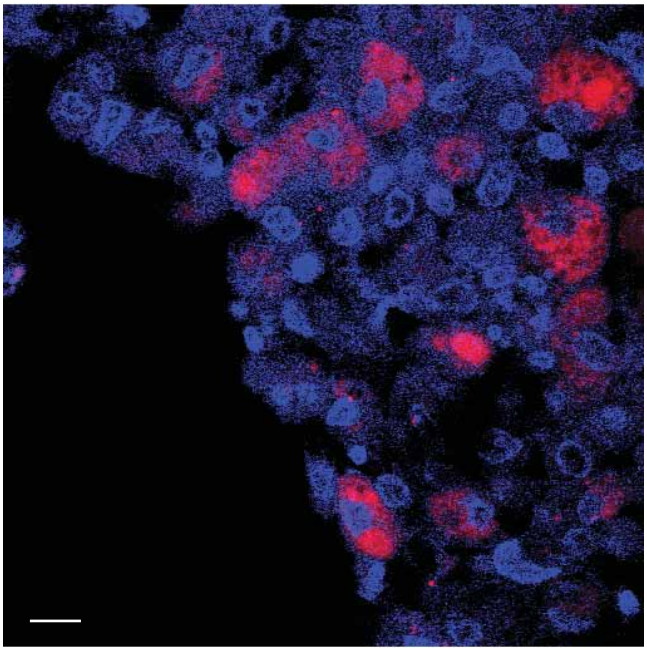

FIGURE 4 *In situ* proximity ligation assay (PLA) demonstrating BRAF–CRAF dimerisation in an *NRAS*^{Q61K}-mutated lesion (patient 23). BRAF–CRAF heterodimerisation was visualised as red dots by *in situ* PLA and was detected with a fluorescent microscope; cell nuclei were stained with 4,6-diamidino-2-phenylindole (blue). Scale bar: 10 µm.

TABLE 4 Univariate analyses of the predictive factors at diagnosis of spontaneous improvement of pulmonary Langerhans cell histiocytosis during follow-up

Parameter at diagnosis	Odds ratio (95% CI)	p-value
Age years	0.95 (0.88–1.03)	0.21
NYHA stage	2.4 (0.91–6.45)	0.08
FEV_1 % pred	0.96 (0.92–1.01)	0.10
***BRAF* status**	0.39 (0.08–1.9)	0.24
***NRAS* status**	0.19 (0.03–1.03)	0.05
***BRAF* and *NRAS* status**	0.1 (0.01–0.98)	0.048

NYHA: New York Heart Association; FEV_1: forced expiratory volume in 1 s.

Discussion

In the present study, we confirmed that the MAPK signalling pathway was constantly activated in PLCH lesions, as previously demonstrated in nonpulmonary LCH specimens [6]. This activation could be explained by the presence of the $BRAF^{V600E}$ somatic mutation in 50% of the lung LCH biopsies studied. This prevalence is in accordance with that observed in previous studies [6–12]. We also identified the presence of the $MAP2K1^{C121S}$ mutation, which may account for MAPK pathway activation in 20% of *BRAF* WT PLCH lesions.

The major finding of our study is the presence of recurrent $NRAS^{Q61K/R}$ mutations (*i.e.* mutations occurring across multiple independent lesions) in 40% of PLCH specimens using both standard pyrosequencing and highly sensitive E-*ice*-COLD-PCR. It should be stressed that $NRAS^{Q61K/R}$ mutations initially detected only by E-*ice*-COLD-PCR were easily identified by pyrosequencing when the genotyping was specifically focused on separate CD1a-positive areas, strongly suggesting that *NRAS* mutant alleles were harboured by PLCH cells. Consistently, using E-*ice*-COLD-PCR, we could not detect *NRAS* mutations in the surrounding lung tissue containing <1% CD1a-positive cells of $NRAS^{Q61K/R}$-mutated PLCH lesions. Finally, we clearly demonstrated that the $NRAS^{Q61R}$ mutated protein was indeed located within CD1a-positive cells.

Although $NRAS^{Q61K/R}$ somatic mutations were reported in Erdheim–Chester disease [30, 31], these mutations have not been previously identified in LCH lesions [6, 14, 15]. Consistently, we did not detect *NRAS* mutations in any of the nonpulmonary LCH lesions analysed, even by E-*ice*-COLD-PCR. Interestingly, in one patient, an $NRAS^{Q61K}$ mutation was identified in the PLCH lesion, whereas no *NRAS* mutation was detected in his skin lesion using the same genotyping techniques. Taken together, the presence of $NRAS^{Q61K/R}$ mutations appears to be a particular feature of LCH lung involvement.

The reason why the two previous studies that performed large targeted genotyping in lesions from patients with PLCH did not detect *NRAS* mutations remains unclear [6, 12]. In addition to the fact that a small number of cases were analysed, heterogeneity within PLCH lesions, as shown in our study, might explain these discrepancies.

Although PLCH occurs almost exclusively in smokers, smoking does not by itself explain the occurrence of *NRAS* mutations. Indeed, we did not detect these mutations in lung samples from smoking controls.

Another important finding of this study is the identification of concurrent $NRAS^{Q61K/R}$ mutations in 50% of $BRAF^{V600E}$-mutated PLCH lesions. Although *BRAF* and *NRAS* mutations are usually mutually exclusive, both mutations were recently identified in multiple myeloma and melanomas, supporting the clonal heterogeneity of these tumours [32–36]. When these two mutations were simultaneously detected, one was at a high frequency and the other at a low frequency [32], which was also the case in most analysed cases of our study. Here, we also demonstrated that *BRAF* and *NRAS* mutations could be present in different areas within the same lung biopsy, clearly demonstrating that different clones of cells harboured either *NRAS* and/or *BRAF* mutations. In this regard, whereas CD1a-positive cells infiltrating nonpulmonary LCH lesions were shown to be of clonal origin [37], Yousem *et al.* [38] demonstrated that these cells were polyclonal in most cases of PLCH. The results of the present study further support the polyclonal nature of LCH cells in PLCH.

In the univariate analyses, the patients whose lesions contained concurrent $NRAS^{Q61K/R}$ and $BRAF^{V600E}$ mutations, but not an $NRAS^{Q61K/R}$ or $BRAF^{V600E}$ mutation alone, exhibited poorer spontaneous outcomes. Additional studies on a larger series of PLCH patients are needed to confirm this finding, as this association was erased in the multivariate analysis.

 DOI: 10.1183/13993003.01677-2015

The discovery of *BRAF*^{V600E} in LCH lesions paved the way for the use of BRAFi (*e.g.* vemurafenib) treatment in progressive cases [13, 39, 40]. The fact that PLCH lesions with *NRAS* mutations exhibit activation of both MAPK and AKT pathways underlines the need for prudent use of BRAFi treatment in patients whose PLCH lesions are concomitantly mutated for both *BRAF* and *NRAS*, as resistance or paradoxical disease progression may occur [28, 29]. Resistance mechanisms acquired during BRAFi treatment have been shown to involve multiple signalling pathways, including *NRAS* mutations [28, 29]. In this regard, the co-occurrence of both *BRAF*^{V600E}- and *NRAS*^{Q61K}-activating mutations was demonstrated in cells derived from patients with melanoma who experienced progressive disease under vemurafenib treatment [28]. In cells with sufficient levels of RAS activation, RAF forms activated dimers. BRAFi binding to one member of the RAF dimer results in the transactivation of the other and induces the activation of ERK signalling, thereby stimulating tumour proliferation [41].

In summary, this study provides further insights into MAPK pathway activation in LCH. Our findings also emphasise the importance of *NRAS* genotyping of PLCH lesions. Patients with a PLCH harbouring a *NRAS* mutation may benefit from MEK inhibitor (MEKi) treatment [42] or alternatively from a combined treatment with a BRAFi and MEKi in dual *BRAF*/*NRAS*-mutated cases, as recently suggested [43].

Acknowledgements

The authors thank Dr Giorgia Egidy-Maskos (INRA, Jouy en Josas, France) for pERK and pAKT IHC; Silvina Dos Reis Tavares, Aurélie Sadoux, Maeva Valluci and Farah Khayati (Hôpital Saint-Louis, Paris, France) for technical support; the Hôpital Saint-Louis Tumour Biobank for managing patient biological samples; and Elisabeth Savariau (Institut Universitaire d'Hématologie, Service d'Infographie, Hôpital Saint-Louis, Paris, France) for her assistance with the figures.

References

1 Weitzman S, Egeler RM. Langerhans cell histiocytosis: update for the pediatrician. *Curr Opin Pediatr* 2008; 20: 23–29.
2 Suri H, Yi ES, Nowakowski GS, *et al.* Pulmonary Langerhans cell histiocytosis. *Orphanet J Rare Dis* 2012; 7: 16.
3 Tazi A, de Margerie C, Naccache JM, *et al.* The natural history of adult pulmonary Langerhans cell histiocytosis: a prospective multicentre study. *Orphanet J Rare Dis* 2015; 10: 30.
4 Tazi A, Marc K, Dominique S, *et al.* Serial computed tomography and lung function testing in pulmonary Langerhans' cell histiocytosis. *Eur Respir J* 2012; 40: 905–912.
5 Rollins BJ. Genomic alterations in Langerhans cell histiocytosis. *Hematol Oncol Clin North Am* 2015; 29: 839–851.
6 Badalian-Very G, Vergilio JA, Degar BA, *et al.* Recurrent *BRAF* mutations in Langerhans cell histiocytosis. *Blood* 2010; 116: 1919–1923.
7 Berres ML, Lim KP, Peters T, *et al. BRAF-V600E* expression in precursor versus differentiated dendritic cells defines clinically distinct LCH risk groups. *J Exp Med* 2014; 211: 669–683.
8 Chilosi M, Facchetti F, Calio A, *et al.* Oncogene-induced senescence distinguishes indolent from aggressive forms of pulmonary and non-pulmonary Langerhans cell histiocytosis. *Leuk Lymphoma* 2014; 55: 2620–2626.
9 Roden AC, Hu X, Kip S, *et al. BRAF V600E* expression in Langerhans cell histiocytosis: clinical and immunohistochemical study on 25 pulmonary and 54 extrapulmonary cases. *Am J Surg Pathol* 2014; 38: 548–551.
10 Sahm F, Capper D, Preusser M, *et al. BRAF V600E* mutant protein is expressed in cells of variable maturation in Langerhans cell histiocytosis. *Blood* 2012; 120: e28–e34.
11 Satoh T, Smith A, Sarde A, *et al. B-RAF* mutant alleles associated with Langerhans cell histiocytosis, a granulomatous pediatric disease. *PLoS One* 2012; 7: e33891.
12 Yousem SA, Dacic S, Nikiforov YE, *et al.* Pulmonary Langerhans cell histiocytosis: profiling of multifocal tumors using next-generation sequencing identifies concordant occurrence of *BRAF* V600E mutations. *Chest* 2013; 143: 1679–1684.
13 Hyman DM, Puzanov I, Subbiah V, *et al.* Vemurafenib in multiple nonmelanoma cancers with *BRAF* V600 mutations. *N Engl J Med* 2015; 373: 726–736.
14 Brown NA, Furtado LV, Betz BL, *et al.* High prevalence of somatic *MAP2K1* mutations in *BRAF V600E*-negative Langerhans cell histiocytosis. *Blood* 2014; 124: 1655–1658.
15 Chakraborty R, Hampton OA, Shen X, *et al.* Mutually exclusive recurrent somatic mutations in *MAP2K1* and *BRAF* support a central role for ERK activation in LCH pathogenesis. *Blood* 2014; 124: 3007–3015.
16 Nelson DS, van Halteren A, Quispel WT, *et al. MAP2K1* and *MAP3K1* mutations in Langerhans cell histiocytosis. *Genes Chromosomes Cancer* 2015; 54: 361–368.
17 Nelson DS, Quispel W, Badalian-Very G, *et al.* Somatic activating *ARAF* mutations in Langerhans cell histiocytosis. *Blood* 2014; 123: 3152–3155.
18 Thumar J, Shahbazian D, Aziz SA, *et al.* MEK targeting in *N-RAS* mutated metastatic melanoma. *Mol Cancer* 2014; 13: 45.
19 Charbel C, Fontaine RH, Malouf GG, *et al. NRAS* mutation is the sole recurrent somatic mutation in large congenital melanocytic nevi. *J Invest Dermatol* 2014; 134: 1067–1074.
20 How-Kit A, Lebbe C, Bousard A, *et al.* Ultrasensitive detection and identification of *BRAF* V600 mutations in fresh frozen, FFPE, and plasma samples of melanoma patients by E-*ice*-COLD-PCR. *Anal Bioanal Chem* 2014; 406: 5513–5520.
21 How Kit A, Mazaleyrat N, Daunay A, *et al.* Sensitive detection of *KRAS* mutations using enhanced-*ice*-COLD-PCR mutation enrichment and direct sequence identification. *Hum Mutat* 2013; 34: 1568–1580.
22 Ilie M, Long-Mira E, Funck-Brentano E, *et al.* Immunohistochemistry as a potential tool for routine detection of the *NRAS* Q61R mutation in patients with metastatic melanoma. *J Am Acad Dermatol* 2015; 72: 786–793.
23 Bergeron A, El-Hage F, Kambouchner M, *et al.* Characterisation of dendritic cell subsets in lung cancer micro-environments. *Eur Respir J* 2006; 28: 1170–1177.

24 Boursault L, Haddad V, Vergier B, *et al.* Tumor homogeneity between primary and metastatic sites for BRAF status in metastatic melanoma determined by immunohistochemical and molecular testing. *PLoS One* 2013; 8: e70826.
25 Arnault JP, Mateus C, Escudier B, *et al.* Skin tumors induced by sorafenib; paradoxic RAS–RAF pathway activation and oncogenic mutations of *HRAS*, *TP53*, and *TGFBR1*. *Clin Cancer Res* 2012; 18: 263–272.
26 Boussemart L, Malka-Mahieu H, Girault I, *et al.* eIF4F is a nexus of resistance to anti-BRAF and anti-MEK cancer therapies. *Nature* 2014; 513: 105–109.
27 Weber CK, Slupsky JR, Kalmes HA, *et al.* Active Ras induces heterodimerization of cRaf and BRaf. *Cancer Res* 2001; 61: 3595–3598.
28 Nazarian R, Shi H, Wang Q, *et al.* Melanomas acquire resistance to B-RAF(V600E) inhibition by RTK or N-RAS upregulation. *Nature* 2010; 468: 973–977.
29 Shi H, Hugo W, Kong X, *et al.* Acquired resistance and clonal evolution in melanoma during BRAF inhibitor therapy. *Cancer Discov* 2014; 4: 80–93.
30 Diamond EL, Abdel-Wahab O, Pentsova E, *et al.* Detection of an *NRAS* mutation in Erdheim–Chester disease. *Blood* 2013; 122: 1089–1091.
31 Emile JF, Diamond EL, Helias-Rodzewicz Z, *et al.* Recurrent *RAS* and *PIK3CA* mutations in Erdheim–Chester disease. *Blood* 2014; 124: 3016–3019.
32 Chiappetta C, Proietti I, Soccodato V, *et al.* BRAF and NRAS mutations are heterogeneous and not mutually exclusive in nodular melanoma. *Appl Immunohistochem Mol Morphol* 2015; 23: 172–177.
33 Goel VK, Lazar AJ, Warneke CL, *et al.* Examination of mutations in *BRAF*, *NRAS*, and *PTEN* in primary cutaneous melanoma. *J Invest Dermatol* 2006; 126: 154–160.
34 Larkin JMG, Yan Y, McArthur GA, *et al.* Update of progression-free survival (PFS) and correlative biomarker analysis from coBRIM: Phase III study of cobimetinib (cobi) plus vemurafenib (vem) in advanced *BRAF*-mutated melanoma. *J Clin Oncol* 2015; 33: 15 Suppl., 9006.
35 Lohr JG, Stojanov P, Carter SL, *et al.* Widespread genetic heterogeneity in multiple myeloma: implications for targeted therapy. *Cancer Cell* 2014; 25: 91–101.
36 Siroy AE, Boland GM, Milton DR, *et al.* Beyond $BRAF^{V600}$: clinical mutation panel testing by next-generation sequencing in advanced melanoma. *J Invest Dermatol* 2015; 135: 508–515.
37 Willman CL, Busque L, Griffith BB, *et al.* Langerhans'-cell histiocytosis (histiocytosis X) – a clonal proliferative disease. *N Engl J Med* 1994; 331: 154–160.
38 Yousem SA, Colby TV, Chen YY, *et al.* Pulmonary Langerhans' cell histiocytosis: molecular analysis of clonality. *Am J Surg Pathol* 2001; 25: 630–636.
39 Charles J, Beani JC, Fiandrino G, *et al.* Major response to vemurafenib in patient with severe cutaneous Langerhans cell histiocytosis harboring *BRAF* V600E mutation. *J Am Acad Dermatol* 2014; 71: e97–e99.
40 Haroche J, Cohen-Aubart F, Emile JF, *et al.* Reproducible and sustained efficacy of targeted therapy with vemurafenib in patients with BRAFV600E-mutated Erdheim–Chester disease. *J Clin Oncol* 2015; 33: 411–418.
41 Callahan MK, Rampal R, Harding JJ, *et al.* Progression of RAS-mutant leukemia during RAF inhibitor treatment. *N Engl J Med* 2012; 367: 2316–2321.
42 Kee D, McArthur G. Targeted therapies for cutaneous melanoma. *Hematol Oncol Clin North Am* 2014; 28: 491–505.
43 Abdel-Wahab O, Klimek VM, Gaskell AA, *et al.* Efficacy of intermittent combined RAF and MEK inhibition in a patient with concurrent BRAF- and NRAS-mutant malignancies. *Cancer Discov* 2014; 4: 538–545.

DOI: 10.1183/13993003.01677-2015